Journal of Materials Chemistry B

Accepted Manuscript

ROYAL SOCIETY OF CHEMISTRY

www.rsc.org/materialsB

Journal of
Materials Chemistry B

COMMUNICATION

Three Dimensional Multipod Superstructure based on $Cu(OH)_2$ as a Highly Efficient Nanozyme

Received 00th January 20xx,
Accepted 00th January 20xx

DOI: 10.1039/x0xx00000x

www.rsc.org/

Ren Cai,[a] Dan Yang,[c] Xigao Chen,[a] Yun Huang,[a] Yifan Lyv,[a,b] Jinglin He,[a,d] Muling Shi,[a,b] I-Ting Teng,[a] Shuo Wan,[a] Weijia Hou,[a] and Weihong Tan[a,b]*

A highly efficient nanozyme system, termed hollow multipod $Cu(OH)_2$ superstructure (HMPS), has been developed via direct conversion from irregular nanoparticles. The HMPS displayed body size around 150 nm and branch lengths in the range of 150~250 nm. Based on the excellent catalytic property of HMPS, we developed a simple and highly sensitive colorimetric assay to detect urine glucose, and the results are in good agreement with hospital examination reports.

Nanomaterial-based enzyme mimetics, called nanozymes, have attracted considerable interest by their unique properties, such as high stability, low cost, and excellent catalytic activity.[1] In particular, materials with three-dimensional (3D) hierarchical superstructures exhibit excellent performance in applications, including drug delivery, live cell imaging, and theranostic application.[2] The individual properties of the building blocks are preserved, and the presence of the secondary architecture also contributes to performance, i.e., chemical stability, uniform porosity, and resistance to aggregation of nanomaterials, all of which can be improved in 3D superstructures.[3] Self-assembly is a powerful approach to create these unique superstructures.[4] For example, uniform twinning superstructures connected by pairs of parallel ZnSe nanorods were generated by a self-limited assembly process.[5] Helical Fe_3O_4 superstructures were obtained through template-free self-assembly of magnetite.[6] Crosslinking dimers with well-controlled interparticle distance and relative orientation were prepared through self-assembly of Au nanodumbbell building blocks.[7] However, these processes may involve relatively weak hydrogen bonds, dipole-dipole or Van der Waals interactions between the subunit components,[8] which, in turn, limit the stability, integrity and application of superstructures.[9]

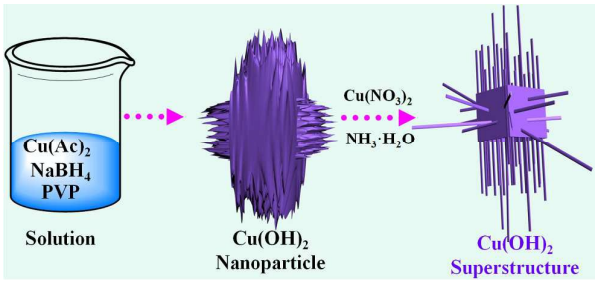

Scheme 1. Schematic illustration of the synthesis process of 3D $Cu(OH)_2$ multipod superstructures.

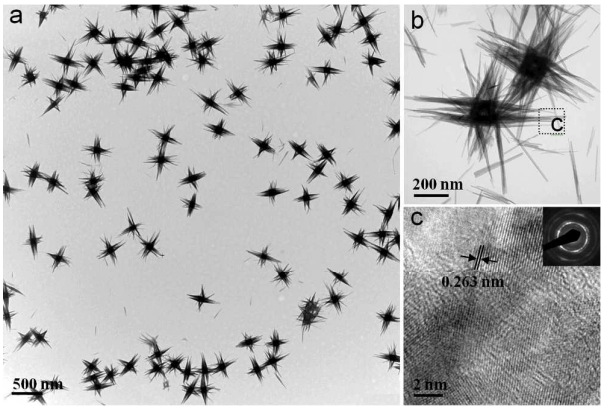

Figure 1. Characterization of 3D $Cu(OH)_2$ multipod superstructures: a) low-magnification and b) high-magnification TEM images; c) HRTEM image (inset is SAED).

Here, we reported the development of a facile process for the preparation of hollow multipod $Cu(OH)_2$ superstructures (HMPS). These superstructures, which are composed of many tiny branches, are transformed at room temperature from $Cu(OH)_2$ nanoparticle (NP) precursors (**Scheme 1**). Benefited from the large surface area and unique configuration endowed by the 3D superstructure, these HMPS offer more active sites to trap the reactive molecules inside and increased the collision probability between these active molecules. This results in a high catalytic activity towards 3,3',5,5'-tetramethylbenzidine (TMB) and H_2O_2. Based on their excellent catalytic activity, we developed a simple colorimetric assay with high sensitivity (limit of detection = 1 nM) to

[a] R. Cai, X. Chen, Y. Huang, Y. Lyv, L. Zhang, J. He, M. Shi, , I. Teng, S. Wan, W. Hou and Prof. W. Tan, Department of Chemistry and Department of Physiology and Functional Genomics, Center for Research at the Bio/Nano Interface, Shands Cancer Center, UF Genetics Institute, McKnight Brain Institute, University of Florida, Gainesville, FL 32611-7200 (USA), Fax: (+1)352-846-2410. E-mail: tan@chem.ufl.edu

[b] Y. Lyv, M. Shi, Prof. W. Tan, Molecular Sciences and Biomedicine Laboratory, State Key Laboratory for Chemo/Biosensing and Chemometrics, College of Chemistry and Chemical Engineering and College of Biology, Collaborative Innovation Center for Molecular Engineering and Theranostics, Hunan University, Changsha 410082, China.

[c] D. Yang, Department of Chemistry, National University of Singapore, 117574 Singapore.

[d] J. He, School of Chemistry and Biological Engineering, Changsha University of Science and Technology, 410004, China

† Footnotes relating to the title and/or authors should appear here.
Electronic Supplementary Information (ESI) available: TEM, XRD, FTIR, UV/Vis, selectivity analysis, hospital examination reports. See DOI: 10.1039/x0xx00000x

detect urine glucose, and the results stand in good agreement with hospital examination reports.

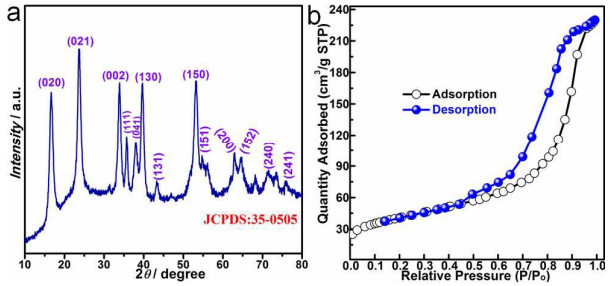

Figure 2. a) XRD patterns and b) Nitrogen gas adsorption and desorption isotherms of the HMPS. The BET surface area is 136.8 m^2/g.

In a typical procedure, amorphous $Cu(OH)_2$ NPs (**Figure S1-S3** in ESI†) and polyvinylpyrrolidone (PVP) were mixed by sonification. Then, certain amount of $Cu(NO_3)_2$ and $NH_3 \cdot H_2O$ was added to the above solution under vigorous stirring. After stirring at room temperature for 15 minutes, the resulting products were collected by centrifugation (see details in the Experimental Section in ESI†). Based on low-magnification transmission electron microscopy (TEM), three-dimensional (3D) architectures with average edge length around 350 nm were formed (**Figure 1a**). High-magnification TEM (**Figure 1b**) images further revealed that these architectures are hollow and composed of many tiny branches with lengths ranging from 150 to 250 nm. The crystal phase of the superstructure was attributed to Cu $(OH)_2$ (JCPDS card no. 35-0505) based on the corresponding powder X-ray diffraction (XRD) pattern shown in **Figure 2a**. The observed lattice fringe of 0.263 nm in the high resolution TEM (HRTEM) image (**Figure 1c**) corresponds to the d spacing of the (002) lattice planes in orthorhombic $Cu(OH)_2$. The ring-type selected-area electron diffraction (SAED) pattern (inset in **Figure 1c**) indicates the polycrystalline nature of these hollow multipod $Cu(OH)_2$ superstructures (HMPS). To investigate the specific surface area, full nitrogen sorption isotherms of the HMPS were measured. According to the Brunauer-Emmett-Teller (BET) model and the data in **Figure 2b**, the specific surface area of the HMPS was 136 m^2g^{-1}.

The formation mechanism of HMPS is illustrated in **Scheme 1** and **Figure S4** (ESI†). When the mixture of $Cu(NO_3)_2$ and $NH_3 \cdot H_2O$ is added to $Cu(OH)_2$ NPs, surface hydrated copper ions (i.e. $[Cu(H_2O)_6]^{2+}$) coordinate with $NH_3 \cdot H_2O$ to generate $[Cu(NH_3)_n]^{2+}$ ($[Cu(H_2O)_6]^{2+} + n\ NH_3 \cdot H_2O \rightleftharpoons [Cu(NH_3)_n]^{2+} + (n+6)\ H_2O$, $NH_3 \cdot H_2O \rightleftharpoons NH_4^+ + OH^-$) (**Figure S4a**, ESI†). However, generated OH^-, which has much stronger affinity than NH_3 to coordinate with Cu^{2+} ions, replaces NH_3 in $[Cu(NH_3)_n]^{2+}$ to form a chain structure on the particle surface,[10] i.e., $[Cu(NH_3)_n]^{2+} \rightarrow [Cu(NH_3)_{n-1}(OH)]^+ \rightarrow [Cu(NH_3)_{n-2}(OH)_2] \rightarrow \ldots\ldots \rightarrow [Cu(OH)_n]^{(n-2)-}$ (**Figure S4b**, ESI†).[11] As a consequence of coordination between OH^- and Cu^{2+}, the chain structure in **Figure S4b** evolves into a one-dimensional (1D) structure (tiny branches) (**Figure S1c-d**, ESI†).[12] Meanwhile, Cu migrates from the inner NPs to the surface,[11] leaving a faintly cavity in the original NPs (**Figure S4c**, ESI†) and forming tiny branches on the surface. Further increase of $NH_3 \cdot H_2O$ solution to 800 µL resulted in slight breakage of tiny branch in the superstructures, in which some branches were dissociated and cavities were visible at the center (**Figure S1e-f**, ESI†).

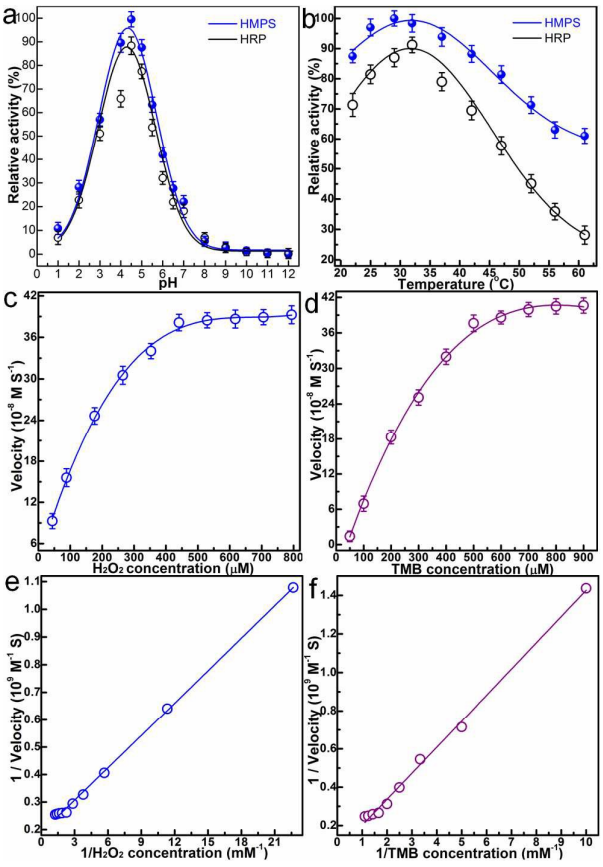

Figure 3. a) and b) the peroxidase-like activities of HMPS and HRP are pH- and temperature- dependent. a) HMPS shows an optimal pH of 4.5; b) HMPS shows an optimal temperature around 25 °C, respectively. Experiments were carried out using 30 µg HMPS or 300 ng HRP in a reaction volume of 0.5 ml, in 0.2 M NaAc buffer, with 800 µM TMB as substrate. H_2O_2 concentration was 530 µM for HMPS and HRP. The maximum point in each curve (a-b) was set as 100%. Steady-state kinetic assays and catalytic mechanism of HMPS: c) The H_2O_2 concentration was 530 µM, and TMB concentration varied. d) The TMB concentration was 800 µM, and H_2O_2 concentration varied. e) and f) Double-reciprocal plots for HMPS with the concentration of e) H_2O_2 fixed and TMB varied and f) TMB fixed and H_2O_2 varied.

Nanozymes are always of great interest in biomimetic chemistry. They possess many unique advantages, such as low cost, high operational stability, facile preparation, and tunable catalytic activity.[13,14] With the large surface area endowed by the 3D superstructure (**Figure 2b**), these HMPS nanozymes offer more active sites and increased collision probability between active molecules trapped inside. For the first set of experiments, we investigated whether these HMPS could mimic peroxidase activity for H_2O_2 and 3,3',5,5'-tetramethylbenzidine (TMB) (**Scheme 2**). As shown in our experiment, HMPS rapidly catalyzed the reduction of H_2O_2 in the presence of TMB, generating blue oxidized TMB within 3 minutes at room temperature (**Figure S5**, ESI†), which in other word, indicating excellent catalytic capability. Next, to decide whether the catalytic activity of HMPS shows similar pH and temperature dependence with that of natural enzymes, we tested catalytic activity of HMPS while varying the pH from 1 to 12 and

the temperature from 22 °C to 65 °C, respectively. For comparison, the activity of horseradish peroxidase (HRP), one of the most utilized natural enzymes for biocatalysis,[15] was also tested (**Figure 3a-b**).[16] As shown in **Figure 3a-b,** high catalytic activity (above 85%) can be achieved with pH in the range of 4 to 5 and temperature in the range of 25 °C to 40 °C. The optimum pH and temperature for HMPS catalysis are approximately 4.5 and 25 °C, respectively, which are very close to for the values obtained from HRP (**Figure 3a-b**).

Table 1 Comparison of the kinetic parameters of HMPS and HRP. K_m is the Michaelis constant, and V_{max} is the maximal reaction velocity.

	Substrate	K_m(mM)	V_{max} (10^{-8} M S^{-1})
HMPS	TMB	1.335	42.1
HMPS	H_2O_2	0.379	39. 1
HRP[19]	TMB	0.434	10
HRP[19]	H_2O_2	3.700	8.71

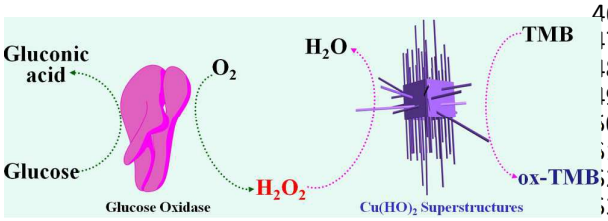

Scheme 2. Schematic illustration of colorimetric detection for glucose by using HMPS-catalyzed reactions.

To provide further insight, the catalytic activity of HMPS was studied by enzyme kinetics theory and methods.[16,17] Typical Michaelis-Menten curves (**Figure 3c-d**) were obtained from a series of TMB or H_2O_2 concentrations and fitted by the Lineweaver-Burk equation (**Figure 3e-f**).[15] Important enzyme kinetic parameters, such as the Michaelis-Menten constant (K_m) and maximum initial velocity (V_{max}), were obtained and are listed in **Table 1**. K_m is an indicator of enzyme affinity to substrate,[18] with a high K_m value representing weak affinity and vice versa. With H_2O_2 as the substrate, the apparent K_m value is about 10 times lower than that of HRP,[19] and the V_{max} is about 5 times larger, indicating better affinity of HMPS to H_2O_2 than that of HRP. This can be ascribed to the high surface area-to-volume ratio in HMPS, which leads to more active sites for H_2O_2,[20] and in turn, results in a lower K_m and a higher V_{max} (**Table 1**). **Figure 4a** shows a concentration-response curve for H_2O_2 detection using HMPS as an artificial enzyme under optimal conditions (i.e., pH 4.5, 25 °C). The linear range is from 0.1 nM to 100 nM in the calibration curve (inset in **Figure 4a**), indicating a low detection limit of 0.1 nM for H_2O_2. In addition, H_2O_2 is the main product of glucose oxidase-catalyzed reactions.[21] Since HMPS has higher catalytic activity and sensitivity for H_2O_2 compared to HRP, colorimetric detection of glucose can be realized using the HMPS-catalyzed reduced reaction of H_2O_2 (**Scheme 2**). Glucose detection can be performed in two steps: (1) glucose-oxidase catalyzes oxidation of glucose to generate gluconic acid and H_2O_2 in presence of oxygen ($\text{Glucose} + O_2 \xrightarrow{\text{Glucose oxidase}} \text{Gluconic acid} + H_2O_2$); (2) then, H_2O_2 is detected by HMPS in the presence of TMB ($H_2O_2 + \text{TMB} \xrightarrow{\text{HMPS}} H_2O + \text{ox-TMB}$).

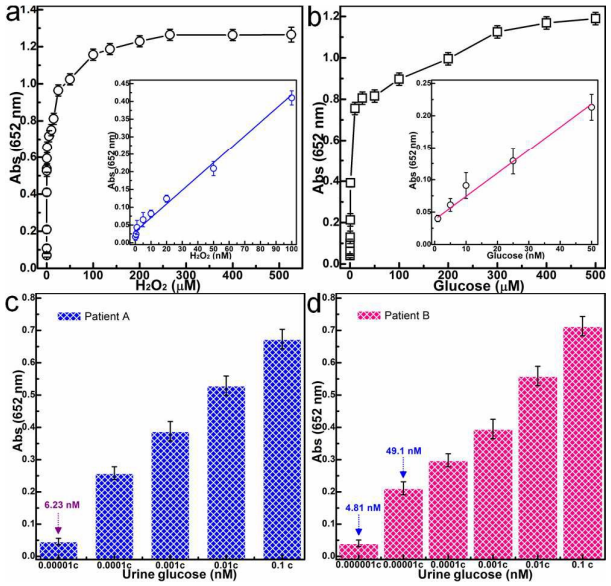

Figure 4. a) Dose-response curve for H_2O_2 detection using HMPS as an artificial enzyme (Inset: linear calibration plot for H_2O_2 detection); b) a dose-response curve for glucose using glucose oxidase and HMPS as an artificial enzyme (Inset: linear calibration plot for glucose detection); c) and d) Analyte concentrations of urine glucose determined by monitoring the absorbance changes at 652 nm for different samples after incubation with glucose oxidase and HMPS. c) Urine samples from Patient A were diluted 10-, 10^2-, 10^3-, 10^4- and 10^5-fold. d) Urine samples from Patient B were diluted 10-, 10^2-, 10^3-, 10^4-, 10^5- and 10^6-fold.

A typical dose-response curve for glucose detection under optimal conditions (i.e., pH 4.5, 25 °C) was shown in **Figure 4b** and the color change during the reaction was shown in **Figure S5** (ESI†). The concentration of glucose that can be detected was as low as 1 nM, and the linear range is from 1 nM to 50 nM (inset in **Figure 4b**). The limit of detection ofglucose by HMPS isaround 1000 times lower than the value for $CoFe_2O_4$ magnetic nanoparticles in a previous report,[22] The selectivity experiments show strong absorbance only for glucose, signals hardly increase in presence of other sugars (**Figure S6**, ESI†), consistent with the high affinity of glucose-oxidase. Low-cost, rapid and noninvasive method to detect glucose for diabetes prevention has always attracted great attention.[23] We attempted to detect glucose in urine stock solution by using the above method in **Figure 4c-d**. According to the calibration curve (inset in **Figure 4b**), the urine glucose concentrations in two patients were 626.72 μM (11.28 mg/dL) and 4.86 mM (87.48 mg/dL), respectively, which are both close to the values reported in clinical examinations (normal, NEG ≤ 100 mg/dL) (**Figure S7-S8**, ESI†). Thus, our colorimetric method based on HMPS offered precise detection of urine glucose of these two patients. Therefore, this colorimetric method shows promise for clinical applications to monitor diabetes.

We have developed a highly efficient nanozyme system, termed 3D hollow multipod superstructure (HMPS), via direct conversion from irregular $Cu(OH)_2$ nanoparticles. The HMPS displayed body size around 150 nm and branch lengths in the range of 150~250 nm. Kinetic analysis indicates that the nanozyme system exhibits much higher catalytic activity to H_2O_2 than that of natural enzyme HRP. The HMPS nanozyme system shows several advantages over HRP,

such as facile preparation, low-cost, and stability. By leveraging the color changes caused by the nanozyme, HMPS can be utilized for the analysis of urine glucose concentration at a low limit of detection (1 nM). Based on these excellent catalytic properties, we developed a simple and highly sensitive colorimetric assay to detect urine glucose, and the results are in good agreement with clinical examination reports. Therefore, the HMPS nanozyme system holds potential in such clinical applications as diabetes monitoring. Furthermore, successful demonstration of this work will facilitate development of more nanozyme systems with high catalytic activity for medical diagnostics.

Acknowledgements

The authors are grateful to Dr. Kathryn Williams for her critical comments during the preparation of this manuscript. This work is supported by grants awarded by the National Institutes of Health (GM079359 and CA133086).This work is also supported by the National Key Scientific Program of China (2011CB911000), NSFC grants (NSFC 21221003 and NSFC 21327009) and China National Instrumentation Program (2011YQ03012412).

Notes and references

1 (a) Y. Lin, J. Ren, X. Qu, *Acc. Chem. Res.* **2014,** *47*, 1097-1105; (b) A. J. Kirby, *Angew. Chem. Int. Ed.* **1996,** *35*, 706-724.

2 (a) L. Qiu, T. Chen, I. Öçsoy, E. Yasun, C. Wu, G. Zhu, M. You, D. Han, J. Jiang, R. Yu, W. Tan, *Nano Lett.* **2015,** *15*, 457-463; (b) O. Chen, L. Riedemann, F. Etoc, H. Herrmann, M. Coppey, M. Barch, C. T. Farrar, J.Zhao, O. T. Bruns, H. Wei, P. Guo, J. Cui, R. Jensen, Y. Chen, D. K. Harris, J. M. Cordero, Z. Wang, A. Jasanoff, D. Fukumura, R. Reimer, M. Dahan, R. K. Jain, M. G. Bawendi, *Nat. Commun.,* **2014**, *5*; (c) N. C. Bigall, C. Wilhelm, M.-L. Beoutis, M. García-Hernandez, A. A. Khan, C. Giannini, A. Sánchez-Ferrer, R. Mezzenga, M. E. Materia, M. A. Garcia, F. Gazeau, A. M. Bittner, L. Manna, T. Pellegrino, *Chem. Mater.* **2013,** *25*, 1055-1062.

3 (a) U. Banin, A. Sitt, *Nat. Mater.* **2012,** *11*, 1009-1011; (b) K. Miszta, J. de Graaf, G. Bertoni, D. Dorfs, R. Brescia,S. Marras, L. Ceseracciu, R. Cingolani, R. van Roij, M. Dijkstra, L. Manna, *Nat. Mater.* **2011,** *10*, 872-876; (c) Y. Xia, T. D. Nguyen, M. Yang, B. Lee, A. Santos, P. Podsiadlo, Z. Tang, S. C. Glotzer, N. A. Kotov, N. A., *Nat. Nano.* **2011,** *6*, 580-587.

4 (a) Z. Sun, T. Liao, Y. Dou, S. M. Hwang, M. S. Park, L. Jiang, J. H. Kim, S. X. Dou, *Nat. Commun.* **2014,** *5*; (b) L. Wang, L. Xu, H. Kuang, C. Xu, N. A. Kotov, *Acc. Chem. Res.* **2012,** *45*, 1916-1926.

5 G. Jia, A. Sitt, G. B. Hitin, I. Hadar, Y. Bekenstein, Y. Amit, I. Popov, U. Banin, *Nat. Mater.* **2014,** *13*, 301-307.

6 G. Singh, H. Chan, A. Baskin, E. Gelman, N. Repnin, P. Král, R. Klajn, *Science* **2014,** *345*, 1149-1153.

7 M. Grzelczak, A. Sánchez-Iglesias, H. H. Mezerji, S. Bals, J. Pérez-Juste, L. M. Liz-Marzán, *Nano Lett.* **2012,** *12*, 4380-4384.

8 (a) Y. Min, M. Akbulut, K. Kristiansen, Y. Golan, J. Israelachvili, J., *Nat. Mater.* **2008,** *7*, 527-538; (b) K. J. M. Bishop, C. E. Wilmer, S. Soh, B. A. Grzybowski, *Small* **2009,** *5*, 1600-1630; (c) K. Liu, N. Zhao, E. Kumacheva, *Chem. Soc. Rev.* **2011,** *40*, 656-671.

9 J. He, Z. Wei, L. Wang, Z. Tomova, T. Babu, C. Wang, X. Han, J. T. Fourkas, Z. Nie, *Angew. Chem. Int. Ed.* **2013,** *52*, 2463-2468.

10 H. Hou, Y. Zhu, Q. Hu, *J. Nanomater.* **2013,** *2013*, 8.

11 X. Wen, W. Zhang, S. Yang, Z. R. Dai, Z. L. Wang, *Nano Lett.* **2002,** *2*, 1397-1401.

12 P. Gao, M. Zhang, Z. Niu, Q. Xiao, *Chem Commun.* **2007,** 48, 5197-5199.

13 Y. Fu, X. Y. Zhao, J. L. Zhang, W. Li, *J. Phys. Chem. C* **2014,** *118*, 18116-18125.

14 H. Wei, E. Wang, *Chem. Soc. Rev.* **2013,** *42*, 6060-6093.

15 H. Deng, W. Shen, Y. Peng, X. Chen, G. Yi, Z. Gao, *Chem. Eur. J.* **2012,** *18*, 8906-8911.

16 L. A. Marquez, H. B. Dunford, *Biochemistry* **1997,** *36*, 9349-9355.

17 Y. Tao, E. Ju, J. Ren, X. Qu, *Adv. Mater.* **2015,** *27*, 1097-1104.

18 Y. Guo, L. Deng, J. Li, S. Guo, E. Wang, S. Dong, *ACS Nano* **2011,** *5*, 1282-1290.

19 L. Gao, J. Zhuang, L. Nie, J. Zhang, Y. Zhang, N. Gu, T. Wang, J. Feng, D. Yang, S. Perrett, X. Yan, *Nat. Nano.* **2007,** *2*, 577-583.

20 R. Cai, D. Yang, S. Peng, X. Chen, Y. Huang, Y. Liu, W. Hou, S. Yang, Z. Liu, W. Tan, *J. Am. Chem. Soc.* **2015,** *137*, 13957-13963.

21 (a) T. Lin, L. Zhong, L. Guo, F. Fu, G. Chen, *Nanoscale* **2014,** *6*, 11856-11862; (b) Y. Song, K. Qu, C. Zhao, J. Ren, X. Qu, *Adv. Mater.* **2010,** *22*, 2206-2210; (c) R. Gill, L. Bahshi, R. Freeman, I. Willner, *Angew. Chem. Int. Ed.* **2008,** *47*, 1676-1679; (d) V. Sanz, S. de Marcos, J. R. Castillo, J. A. Galbán, *J. Am. Chem. Soc.* **2005,** *127*, 1038-1048.

22 W. Shi, X. Zhang, S. He, Y. Huang, *Chem Commun* **2011,** *47*, 10785-10787.

23 (a) X. Sun, T. D. James, *Chem. Rev.* **2015,** *115*, 8001-8037; (b) Y. Xu, W. Zhao, W. Wang, Y. Bi, J. Li, S. Mi, M. Xu, J. Lu, T. Wang, M. Li, Z. Wang, Y. Jiang, L. Wang, L. Wang, M. Dai, D. Zhang, S. Lai, G. Ning, *J. Diabetes* **2015**, DOI: 10.1111/1753-0407.12305;(c) P. Mascarenhas, B. Fatela, I. Barahona, *Plos One* **2014,** *9*, e101706.

TOC